Nonlinear imaging of damage in composite structures using sparse ultrasonic sensor arrays

F. Ciampa[1], Simon G. Pickering[1], Gennaro Scarselli[2], M. Meo[1*]

[1]Materials Research Centre, Department of Mechanical Engineering, University of Bath, Bath BA2 7AY, UK

[2]Department of Engineering for Innovation, University of Salento, Via per Monteroni (Lecce), 73100, Italy

Abstract

In different engineering fields, there is a strong demand for diagnostic methods able to provide detailed information on material defects. Low velocity impact damage can considerably degrade the integrity of structural components and, if not detected, can result in catastrophic failures. This paper presents a nonlinear structural health monitoring imaging method, based on elastic wave spectroscopy, for the detection and localisation of nonlinear signatures on a damaged composite structure. The proposed technique relies on the bispectral analysis of ultrasonic waveforms originated by a harmonic excitation and it allows for the evaluation of second order material nonlinearities due to the presence of cracks and delaminations. This nonlinear technique was combined with a radial basis function approach in order to achieve an effective visualisation of the damage over the panel using only a limited number of acquisition points. The robustness of bispectral analysis was experimentally demonstrated on a damaged carbon fibre reinforced plastic (CFRP) composite panel, and the nonlinear

* Corresponding author: m.meo@bath.ac.uk

source's location was obtained with a high level of accuracy. Unlike other ultrasonic imaging methods for damage detection, this methodology does not require any baseline with the undamaged structure for the evaluation of the defect, nor a priori knowledge of the mechanical properties of the specimen.

Keywords: Nonlinear Acoustics, Imaging Methods, Bicoherence Analysis, Radial Basis Functions, Delaminations.

1 Introduction

In the aerospace field and in many other engineering applications, structural health monitoring (SHM) imaging techniques based on ultrasonic wave propagation have attracted the interest of scientists and engineers as they can provide key information regarding the structural characteristics and the residual life of a component [1], [2], [3] and [4]. Indeed, SHM methods are becoming more and more reliable, so that damage tolerance criteria play a challenging role in mitigating structural failures due to fatigue in aircraft structural design. Literature provides a quantitative number of diagnostic imaging methods that can continuously provide a detailed image of the structural damage. Most of them are based on the linear elastodynamic theory and measure the reflection and scattering of primary waves at the material heterogeneities and discontinuities. One type of imaging technique is the *elliptical* or *sum-and-delay* method [5], wherein differenced waveforms (i.e. residual signals from the difference between damaged and undamaged states) acquired by all transducer pairs are summed for each spatial point (i.e. time delay) of the image. For a single sensor pair, this imaging process maps a single echo to an ellipsis with its foci being the transmitter/receiver locations. As

additional pairs are added, the ellipses intersect at the defect location thus reinforcing the signal. A second algorithm, known as the *energy arrival technique* [6], is an adaptively windowed version of the *elliptical* method. This has the effect of reducing the amplitude of the edge reflections, improving the quality of the image. However, all these algorithms rely on the availability of a baseline (undamaged structure) and the time origin of the excitation, as well as a known group velocity for the elastic waves. Over the past 30 years, the *migration technique* was applied to SHM systems in order to recover the location and shape of reflecting, refracting and diffracting defects. This method, derived from geophysics, is based on the idea that reconstruction of the image can be made via numerical finite difference calculations. The signals recovered by the receivers (positioned along a line including the emitter sensor) are time-reversed and back-propagated to create image snapshots of the displacement field, in particular at the moment at which all back-propagated waves precisely converge on the defect [7]. Initially this technique was limited only to isotropic materials, however this methodology has been extended to anisotropic composite laminates in which the group velocity was taken as a function of the propagation direction [8]. In the last few years, ultrasonic nonlinear methods have stimulated interest in the SHM community due to their high sensitivity to detect damage in structures where the crack size is comparable with the ultrasonic wavelength (e.g. micro-cracks, contact-type defects, delamination, inclusions, etc…) [9], [10] and [11]. In particular, nonlinear elastic wave spectroscopy (NEWS) methods have shown to be sensitive in discovering structural defects even at an early stage of development [12], [13]. In [14] a NEWS method was used to evaluate the degradation of material properties of a steel structure that had undergone fatigue loading. The generation mechanism of the second order harmonic frequency

components during the propagation of ultrasonic waves through the degraded material was explained by means of classical nonlinear elasticity (CNL) theory [15]. In particular, the classical second order nonlinear parameter β was found to be proportional to the magnitude of the load and the number of fatigue cycles. In [16] a damage detection investigation was carried out based on the observation of the presence of harmonics and sidebands on the spectrum of the recorded signals excited by a bi-tonal harmonic input. In the absence of damage, the signal spectrum did not contain any harmonics or sidebands that, on the contrary, were recorded in the damaged signal spectrum. The proposed approach allowed the presence of damage in a sandwich composite structure to be detected, even when this damage was localised in a small area and it was barely visible from the top surface. Other authors have used the NEWS methods with the aim of developing robust techniques of detection and localization of damage in a variety of samples [17], [18]. In [19], the nonlinear structural response acquired in different locations of the sample in both the time and frequency domain was analysed to evaluate statistical indicators produced by nonlinearities. Solodov et al. [20] developed a fully non-contact nonlinear local defect resonance (LDR) imaging method to detect near-surface and in-depth delamination using laser vibrometry. Finally, Ciampa and Meo [21], [22] developed an imaging method for the visualisation of structural damage in composite structures based on a combination of nonlinear inverse filtering process and phase symmetry analysis.

This paper presents a nonlinear imaging method based on higher order statistic such as bispectral and bicoherence analysis in order to detect and localise the presence of a crack or delamination in a composite laminate. Unlike the standard second order nonlinear parameter β, the bicoherence coefficient was used to study the nonlinear

response of the sample undergoing harmonic excitation, as it exhibited high sensitivity to second order material nonlinearities. Bicoherence provides additional information on the estimation of the damage location through the quadratic phase coupling between the fundamental and second harmonic amplitudes contained in the measured signals [23]. Radial basis function (RBF) interpolation was then used to image the damage location by reducing the number of receiver points, thus simulating a sparse array of receiver sensors [24]. RBF is usually used to reconstruct smooth, manifold surfaces from point-cloud data for computer visualisations [25]. They can also be employed to repair incomplete meshes in large data sets (e.g. in finite element problems) [26], as a mesh simplification tool and remeshing application or to interpolate displacements of boundary nodes with respect to a whole mesh [27]. The experimental results carried out on a carbon fibre reinforced plastic (CFRP) composite laminate showed a strong correlation of the bicoherence with the internal defect location and encouraged the use of higher order statistic and RBF as a nonlinear ultrasonic imaging technique for damage detection using a limited number of receiver sensors. The layout of this paper is as follows: in Section 2, bispectral and bicoherence analysis are theoretically presented. Section 3 illustrates the nonlinear imaging method with the RBF approach. Section 4 reports the experimental set-up, whilst Section 5 shows the results of the nonlinear imaging process. Finally, the conclusions are drawn and summarised.

2 Theoretical Development

In the following Section, the concepts of bispectrum, classical second order nonlinear parameter β and bicoherence will be briefly presented and discussed since they

represent the theoretical basis of the approach followed in this work for the image of the damage location on the composite structure.

2.1 Bispectral Analysis

The most traditionally employed signal processing techniques used to measure the acousto/ultrasonic elastic features of a medium are the first and second-order statistics, such as the mean, variance and power spectrum. The last method in particular, which is the decomposition over frequency of the signal power, is related to the auto-correlation function and is mostly used to describe linear and Gaussian processes [28]. However, power spectral analysis has the drawback of discarding all phase information. Higher order statistics (HOS) such as bispectral analysis, can be seen as a decomposition of the third moment of a signal over frequency, and can be used to measure the magnitude of the even (second) order harmonic frequency components in the propagated ultrasonic waves [29]. Bispectrum is in fact the two-dimensional Fourier Transform of the third order correlation function and is generally complex valued. For a real, zero-mean stationary random process $x(t)$, the power spectral density $P(\omega_m)$ and bispectrum $B(\omega_m,\omega_n)$ are given by [28]:

$$P(\omega_m) = \int_{-\infty}^{+\infty}\int_{-\infty}^{+\infty} R_{xx}(\tau) e^{j\omega_m\tau}\, d\tau \tag{1}$$

$$B(\omega_m,\omega_n) = \int_{-\infty}^{+\infty}\int_{-\infty}^{+\infty} R_{xxx}(\tau_1,\tau_2) e^{j(\omega_m\tau_1+\omega_n\tau_2)}\, d\tau_1 d\tau_2 \tag{2}$$

where $R_{xx}(\tau)$ and $R_{xxx}(\tau_1,\tau_2)$ are the auto-correlation function and third order auto-correlation function of $x(t)$, respectively. By using the statistical expectation operator $E[\cdot]$, Eqs. (1) and (2) can be rewritten as:

$$P(\omega_m)=E\left[X(\omega_m)X^*(\omega_m)\right] \tag{3}$$

$$B(\omega_m,\omega_n)=E\left[X(\omega_m)X(\omega_n)X^*(\omega_m+\omega_n)\right] \tag{4}$$

where $X(\omega_m)$ is the Fourier Transform of the measured signal $x(t)$ and the asterisk sign "*" corresponds to a complex conjugate operation. Therefore, as the power spectrum decomposes the power of a signal, the bispectrum decomposes the third order cumulant by analysing the frequency interaction between the frequency components at ω_m, ω_n and $\omega_m+\omega_n$. However, due to several symmetries in the (ω_m,ω_n) plane, it is not necessary to compute $B(\omega_m,\omega_n)$ for all ω_m and ω_n pairs. Indeed, there exists a non-redundant region called the Principal Domain that is defined as [30]:

$$(\omega_m,\omega_n):\quad 0\le\omega_m\le\frac{2\pi f_s}{2},\quad \omega_n\le\omega_m,\quad 2\omega_m+\omega_n\le 2\pi f_s \tag{5}$$

where f_s is the sampling frequency. In addition, the three frequency components ω_m, ω_n and $\omega_m+\omega_n$ have a special phase relation defined as follows:

$$\phi_k=\phi_m+\phi_n \tag{6}$$

where ϕ_m and ϕ_n are the phases of the signal at frequencies ω_m and ω_n, respectively, and ϕ_k is the phase of the signal at frequency $\omega_m+\omega_n$. This last condition, known as quadratic phase coupling (QPC) [31], results from the second order nonlinearity due to structural damage, and it can be considered as the bispectrum's ability to detect nonlinear elastic features within the medium. In other words, if conditions (5) and (6) are satisfied, QPC allows discriminating between the structural nonlinearity that would be quadratic phase coupled and other experimental spurious sources such as ambient and equipment noise that, instead, might not be. Indeed, let us assume that the spectrum of the measured signal $X(\omega)$ is expressed as a superposition of the nonlinear structural

response $U(\omega)$ and random contributions due to the effects of the experimental noise, $\eta_a(\omega)$, and the electronic noise, $\eta_e(\omega)$, [32]:

$$X(\omega)=U(\omega)+\eta_a(\omega)+\eta_e(\omega)=U(\omega_m,\omega_n,\phi_m,\phi_n)+k_a n_a(\omega_q,\phi_q)+k_e n_e(\omega_p,\phi_p) \quad (7)$$

where $n_a(\omega_q,\phi_q)$ and $n_e(\omega_p,\phi_p)$ are random variables of constant amplitude k_a and k_e. Since generally the subscripts $q,p\neq m,n$, both environmental and experimental noise do not allow for QPC. Hence, bispectral analysis can be significantly useful in sensing small high order nonlinear harmonic components induced by the interaction of elastic waves and the material defects. To this purpose, by setting $\omega_m=\omega_n=\omega_1$ and calculating the magnitude of Eqs. (3) and (4), yields:

$$P(\omega_1)=\left|X(\omega_1)X^*(\omega_1)\right|=\left|X(\omega_1)\right|^2 \quad (8)$$

$$B(\omega_1,\omega_1)=\left|X(\omega_1)X(\omega_1)X^*(\omega_1+\omega_1)\right|=\left|X(\omega_1)X(\omega_1)X^*(\omega_2)\right| \quad (9)$$

with $\omega_2=2\omega_1$.

2.2 Estimation of Nonlinear Parameters

According to Landau's nonlinear classical theory [15] and Eq. (8), the standard second order nonlinear parameter β can be obtained as a solution of the nonlinear elastodynamic wave equation via a first order perturbation theory as follows [32]:

$$\beta(\mathbf{r}_m)\propto\frac{\sqrt{P(\omega_2)}}{P(\omega_1)} \quad (10)$$

where $P(\omega_2)$ is the magnitude of the power spectral density associated with the second harmonic frequency component and $\mathbf{r}_m=x_m\hat{i}+y_m\hat{j}$ is the position vector of the m $(1\leq m\leq M)$ receivers located on top surface of the composite panel. The parameter

$\beta(\mathbf{r}_m)$ is herein introduced to quantify the second nonlinear elastic response of a structure subjected to harmonic excitation. An analogous nonlinear parameter can be obtained from the bispectral analysis in order to measure the amount of coupling between the angular frequencies ω_1 and $2\omega_1$. In particular, the bicoherence $b^2(\mathbf{r}_m)$ is a useful normalized form of bispectrum that measures QPC on an absolute scale between zero and one and can be defined as:

$$b^2(\mathbf{r}_m) = \frac{B(\omega_1, \omega_1)^2}{P(\omega_1)P(\omega_1)P(\omega_2)} \tag{11}$$

A value of one in the above equation indicates perfect quadratic phase coupling, whilst a value of zero indicates the absence of phase coupling. Since the bispectrum has a variance proportional to the triple product of the power spectra, it can result in the second order properties of the acquired signal dominating the estimation. The advantage of normalisation within the bicoherence process in Eq. (11) is to make the variance approximately flat across all frequencies [34]. Hence, both the parameter $\beta(\mathbf{r}_m)$ and the bicoherence $b^2(\mathbf{r}_m)$ will be used to characterise the nonlinearity of the structural response of the composite laminate subjected to a harmonic excitation.

3 Nonlinear Imaging Method

In this study, a diagnostic nonlinear imaging method was developed to detect the second order nonlinear response of a damaged composite laminate using two sensors in pitch-catch mode. Both the second order nonlinear parameter $\beta(\mathbf{r}_m)$ and the bicoherence coefficient $b^2(\mathbf{r}_m)$ were used to measure the second order nonlinear elastic effects due the interaction of the elastic waves with the crack interfaces (i.e. due to “clapping and

rubbing motion") [35]. In particular, the damaged zone (i.e. the area on the top surface examined by the receiver sensor, with dimensions 210 mm x 150 mm) surrounding the defect was divided into M = 5 x 7 cells distributed along a grid at intervals of 30 mm (Fig. 1). The structural response was then acquired using a receiver piezoelectric transducer placed in each of the m $(1 \le m \le M)$ cells of the damaged zone.

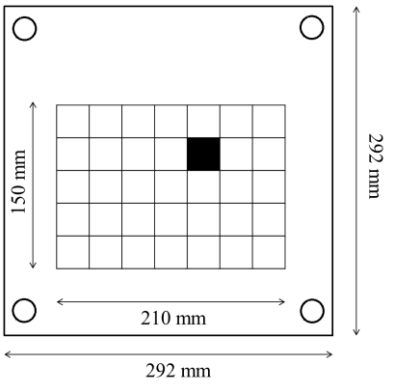

Figure 1 Representation of the damaged zone on the composite panel. The black square corresponds to the damage location. The circles represent the transmitter positions

An excitation a signal consisting of a 5-cycle Hanning-windowed tone burst at 223.5 kHz was generated, amplified and used to drive a transmitter piezoelectric sensor surface bonded to the sample under investigation. Such a fundamental frequency was tuned to find local maxima in the sample response using a swept signal from 150 to 300 kHz, thus fulfilling the QPC condition [Eq. (6)]. Fig. 2 reports the values of bicoherence at the damage location calculated from Eq. (11) for different excitation frequencies.

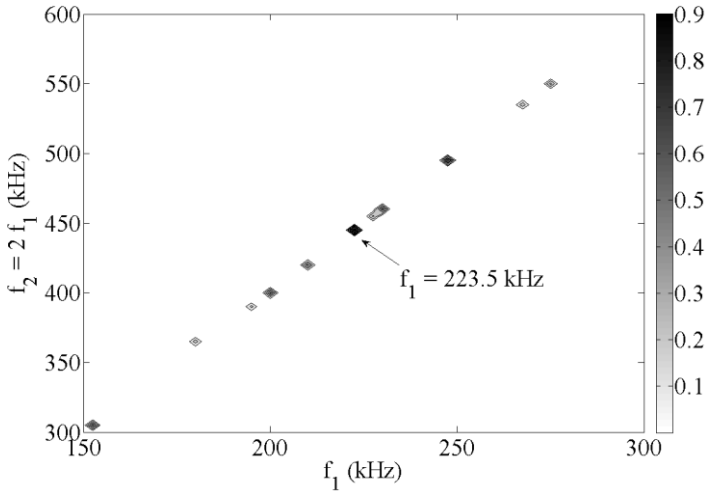

Figure 2 Bicoherence contour plot at the damage location. The maximum value of bicoherence was experimentally obtained at f_1 = 223.5 kHz.

From the above figure, it can be clearly seen that the maximum value of bicoherence was achieved at the input frequency of 223. 5 kHz. According to Eqs. (10) and (11) both values of $\beta(\mathbf{r}_m)$ and $b^2(\mathbf{r}_m)$ were calculated for each cell of the grid and plotted on a 2D map. As the transmitter transducer was moved in N = 4 different positions of the composite plate, two different 2D maps were obtained for $\beta_{tot}(\mathbf{r}_m)$ and $b^2_{tot}(\mathbf{r}_m)$ to retrieve the values of the nonlinear coefficients at the damage location according to:

$$\beta_{tot}(\mathbf{r}_m) = \frac{1}{N}\sum_{k=1}^{N}\beta_k(\mathbf{r}_m) \quad m = 1,\mathrm{K}\ ,M \tag{12a}$$

$$b^2_{tot}(\mathbf{r}_m) = \frac{1}{N}\sum_{k=1}^{N}b^2_k(\mathbf{r}_m) \quad m = 1,\mathrm{K}\ ,M \tag{12b}$$

where N is the number of transmitter positions. Similarly to [36], the number N = 4 was arbitrarily chosen to provide satisfactory results for the damage localisation.

3.1 Nonlinear Imaging with Radial Basis Functions

In the previous Section a multiple sensing element arrangement composed of M cells (i.e. the receiver positions) was used to calculate the 2D maps of the nonlinear coefficients. Hence, in order to reduce the number of cells needed to create an image of the nonlinear second order structural defect, radial basis functions (RBF) interpolation was used. In other words, RBF was employed to highlight the damage location by reducing the number of receiving points, thus simulating a sparse array of receiver sensors. RBF is commonly exploited for scattered data interpolations problems, since it is able to interpolate arbitrary sets of point clouds in a smooth manner [37]. The most popular choices of radial basis functions ϕ are reported in [38]. In this work, the thin-plate spline basis function was used, which can be defined as:

$$\phi(\mathbf{r}) = \mathbf{r}^2 \log \mathbf{r} \tag{13}$$

where $\mathbf{r} = x\hat{i} + y\hat{j}$ is the position vector of each point on the damaged zone (including the points $\mathbf{r}_m$). The thin-plate spline is known a "smoothest" interpolator in the sense that it not only provides C^1 continuity[†] and satisfies the interpolation condition [Eq. (A6)], but also it minimises the energy functional over all the interpolant points for which the energy functional is well defined [Eq. (A7)]. Hence, according to theoretical aspects on RBF reported in the Appendix, the nonlinear values $s_{tot}(\mathbf{r},\mathbf{r}_m)$ in all the points of the damaged zone with coordinate $\mathbf{r}$ can be obtained from Eq. (A16) as follows:

$$s_{tot}(\mathbf{r},\mathbf{r}_m) = \frac{1}{N}\sum_{k=1}^{N} s_k(\mathbf{r},\mathbf{r}_m) \tag{14}$$

[†] The notation C^i is used to denote a function which is continuous in its first i derivatives

Eq. (14) defines a new 2D map in which the location of the damage within the composite structure can be retrieved even reducing the number of receiver points on the damaged zone.

4 Experimental set-up

The experiments were carried out on a composite carbon fibre reinforced plastic (CFRP) plate with dimensions 292 x 292 x 3 mm and a stacking sequence of $[0,90/+-45/0,90/+-45/0,90/+-45]_s$ (Fig. 3).

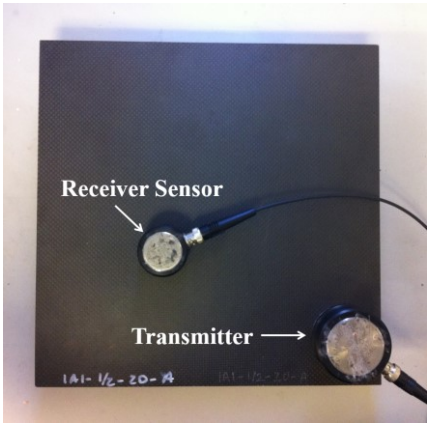

Figure 3 Composite test sample and piezoelectric transducers used in the experiments

To simulate delamination damage, the specimen was fabricated with a 10-mm squared Teflon patch inserted between the plies. The location of the damage was at coordinate x = 135 mm and y = 105 mm within the damaged zone with the origin at the bottom left corner of the grid (Fig. 1). To transmit the waveforms, a 50-mm-diameter Olympus – Panametrics NDT X1020 piezoelectric sensor with a central frequency of 100 kHz was surface bonded on the composite structure using a coupling gel. The transducer was linked to a preamplifier and connected to a National Instrument (NI) data acquisition system consisting of the NI PXI 5421 16-bit arbitrary waveform generator card to send the tone burst at 223.5 kHz. The excited voltage applied was around 250 V in order to

maximize the efficiency of the available transducers. In order to measure the material nonlinear response, a 3-cm-diameter Olympus – Panametrics NDT V101 piezoelectric sensor with a central frequency of 500 kHz was connected to the NI PXI-5105 8-channel digitizer/oscilloscope card (Fig. 4).

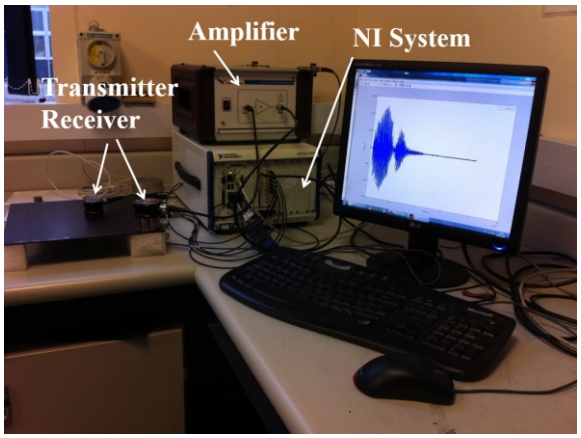

Figure 4 Experimental Set-up

The waveforms acquired in each cell of the damaged zone were Fourier transformed and then averaged across 20 acquisitions in order to reduce the effects of noise contained in the measured signals. Each nonlinear response was sampled at 20 MHz with a total acquisition time of 2 ms. Fig. 5 reports the time history and the associated spectrum of two measured signals, i.e. at the damage location (5a-b) and in a point far from it (5c-d). Whilst the presence of the second harmonic is clearly visible in both signals, its magnitude at the damage location is higher (nearly 25 dB of difference).

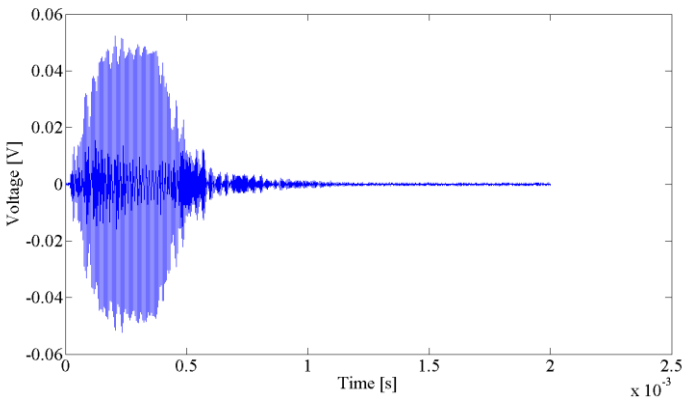

(a)

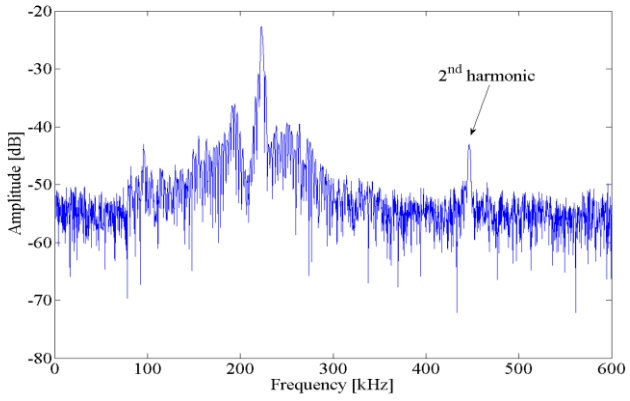

(b)

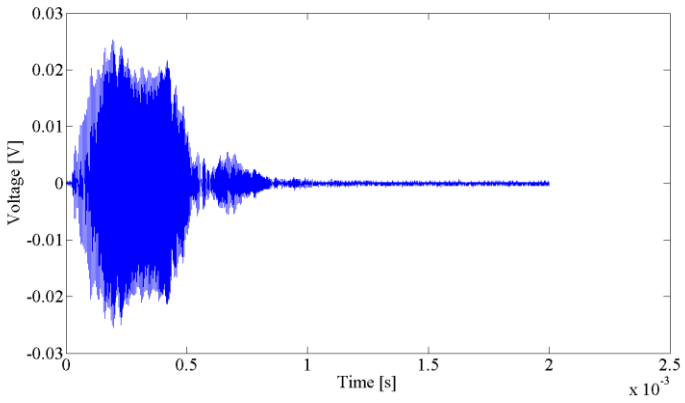

(c)

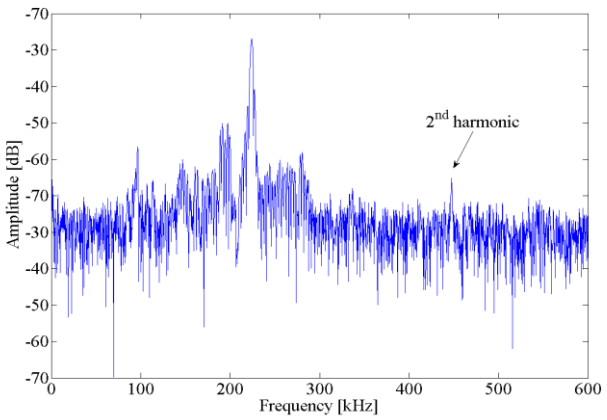

(d)

Figure 5 Time histories and associated Fourier transforms measured at the damage location (a-b) and far from it (c-d).

5 Nonlinear Imaging Results

As explained in Section 3, the acquired second order nonlinear responses were used to obtain an image representative of the damage using the two different nonlinear

parameters, i.e. the second order nonlinear parameter $\beta(\mathbf{r}_m)$ and the bicoherence $b^2(\mathbf{r}_m)$.The envelope of the structural response was first computed using the Hilbert transformation and then, according to Eqs. (12a) and (12b), the damage location was retrieved from a 2D map of each cell of the damaged zone. Fig. 6 represents the resulting image of the damage location created by summing the contributions of all four nonlinear coefficients at each transmitter position.

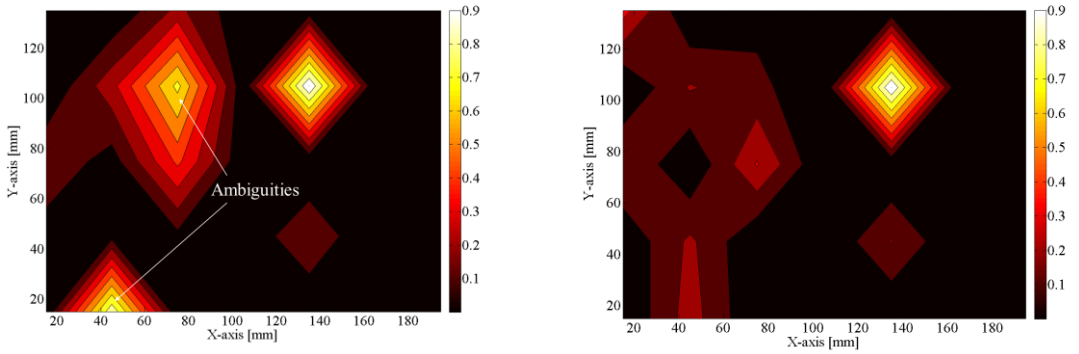

Figure 6 Image of the structural damage using the second order nonlinear coefficient $\beta_{tot}(\mathbf{r}_m)$ (a) and the bicoherence $b^2_{tot}(\mathbf{r}_m)$ (b).

As it can be seen from Fig. 6, the bicoherence coefficient appeared to be very sensitive to the presence of the second order nonlinearities and, compared to $\beta(\mathbf{r}_m)$, it allowed a better estimation of the damage location. This might be due to the lack of information provided by the second order nonlinear coefficient on the quadratic phase coupling between the fundamental and the second harmonic. Indeed, by definition [Eq. (10)], the parameter β does not provide any information of the phase of the measured signals, which may lead to ambiguities in the image of the nonlinear source. According to Eq. (7), such ambiguities could be produced by spurious experimental sources of nonlinearity such as the environmental noise (e.g. the coupling between the receiver and

the composite structure) and the equipment noise. Hence, the bicoherence was able to reveal the presence of damage within the composite laminate only due to second order nonlinearity. The second imaging technique based on RBF was then used to simulate a sparse array of receivers. The following four plots in Fig. 7 were produced by reducing the number of the *M* receiver points on the damaged zone by means of a combination of RBF and $b^2(\mathbf{r}_m)$.

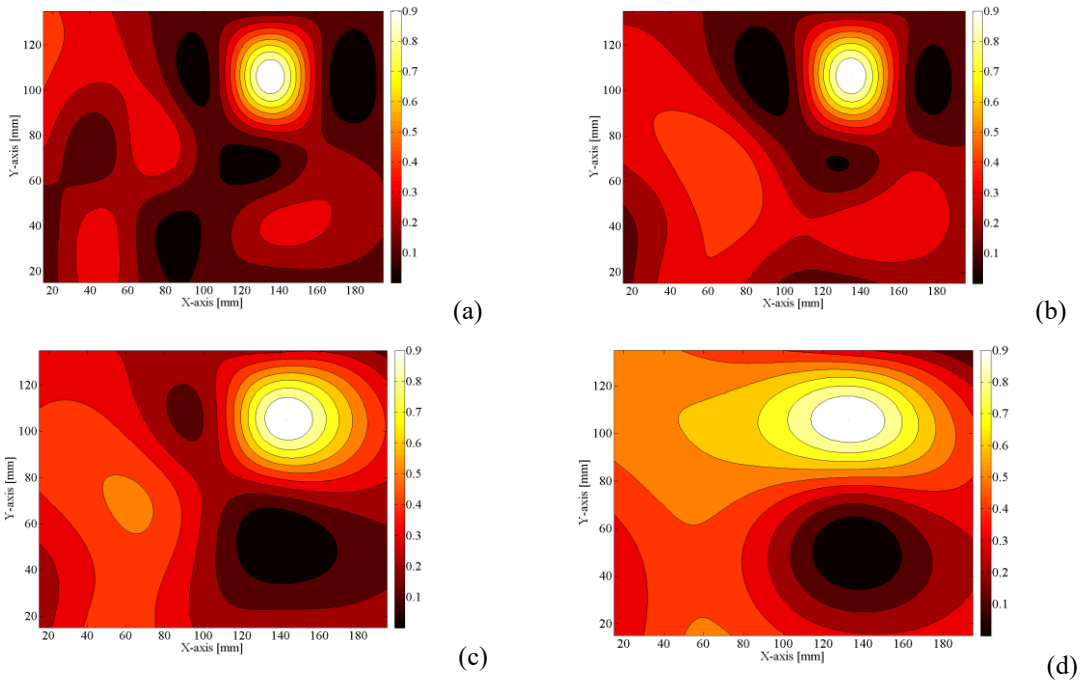

Figure 7. Images of the structural damage using the bicoherence coefficient $b^2(\mathbf{r}_m)$ post-processed through RBF using (a) 35 points; (b) 20 points; (c) 10 points; (d) 6 points.

Once more, according to Eq. (14), the 2D maps were generated as a sum of the RBF contribution of four different transmitter positions. For the RBF implementation, the number of points was decreased from the total 35 points to either 20, 10 or 6 points. In all cases, damage could still be located accurately. It should be noted that only the bispectral analysis results was used in the implementation of the RBF algorithm, as these results did not show any ambiguities due to spurious experimental sources of

nonlinearity. The main conclusion that can be drawn from the Fig. 7 is that RBF effectively allows the localisation of structural damage even using a limited sparse set of acquisition points. These points were randomly chosen over the surface of the panel, ensuring that the point associated with the damage was not included in the RBF evaluation. As expected, by limiting the number of points the predicted extent of the damage increases resulting in a more extended area on the sample in which the damage might be located. Nevertheless, the imaging technique provided useful and accurate results since the actual damage was always included in the predicted area (see values of the 2D maps close to one in Fig. 7). Finally, compared to other ultrasonic imaging techniques, such a nonlinear imaging process requires only simple signal processing to locate the nonlinear source as well as not requiring a priori knowledge of the sample's mechanical properties, dispersion behaviour or a baseline of the undamaged structure.

Conclusions

The paper presents a nonlinear imaging process for the detection and localization of damage in composite structures. The basic principle is that the level of nonlinearity in the elastic response of materials containing structural damage is far greater than in materials with no structural damage. Indeed, nonlinear wave diagnostics of damage are remarkably sensitive to the detection and progression of damage in materials. The sample used for the experimental tests was a square composite panel typical of aerospace applications, inside which a Teflon patch was inserted to simulate delamination damage. By exciting this sample with a harmonic excitation, the resultant spectrum showed a strong nonlinearity represented by the occurrence of the second harmonic nonlinear response caused by delamination. Time domain signals were

processed to obtain the bicoherence values at different locations in the acquisition grid. The experimental results show that compared with the standard classical nonlinear coefficient, the bicoherence produced the most reliable signature for identifying the nonlinear source. Finally, the radial basis function approach was used for imaging the damage on the plate-like sample with a sparse array of acquisition points. Since this nonlinear imaging method does not require any information of the mechanical properties nor the stacking sequence of the composite laminate, future work is ongoing to further optimise the number of transmitter and receiver transducers and demonstrate the capabilities of this nonlinear imaging method on damaged components of larger dimensions and complex geometries.

Appendix

Let us consider a set of points $\{\mathbf{r}_m\}_{m=1}^{M} \in \Omega \subset \Re^n$, with Ω the influence domain (i.e. the damaged zone) and let ϕ be a fixed, real-valued, radially symmetric function on $\Re^n$. RBF interpolation method employs a "radial" function $\phi : \Re^n \to \Re$ to construct the interpolant scalar function *s(**r**)*, i.e. the RBF of the form [38]:

$$s(\mathbf{r}, \mathbf{r}_m) = \sum_{m=1}^{M} \lambda_m \phi\left(\left\|\mathbf{r} - \mathbf{r}_m\right\|\right) + \sum_{j=1}^{N_{poly}} b_j p_j(\mathbf{r}), \qquad \text{(A1)}$$

where $p_j(\mathbf{r})$ is a basis for polynomials of degree at most k (typically linear or quadratic), $\left\|\mathbf{r} - \mathbf{r}_m\right\| = \left[(x - x_m)^2 + (y - y_m)^2\right]^{1/2}$ is the Euclidean norm so that $\phi\left\|\mathbf{r} - \mathbf{r}_m\right\|$ is the basis function centred at $\mathbf{r}_m$ (i.e. receiving point in which the nonlinear values are known), and λ_m and b_j are the weights or the expansion coefficients of the basis functions and the polynomial, respectively. Also, M and N_{poly} denote the number of control points $\boldsymbol{r}_m$ and

the number of polynomial terms, with $M > N_{poly}$. The RBF [Eq. (A1)] consists of a weighted sum of a radially symmetric basis function ϕ located at the centres $\boldsymbol{r}_m$ and a low degree polynomial $p_j(\mathbf{r})$. Given a set on M control points $\boldsymbol{r}_m$ and values $\{f_m\}_{m=1}^{M} \in \Omega \subset \Re$, the process of finding an interpolating RBF s(**r**) for any internal point M of the mesh is called fitting and in matrix form is given by:

$$s(\mathbf{r}, \mathbf{r}_m) = \mathbf{M}^T \boldsymbol{\lambda} + \mathbf{P}^T \mathbf{b} \tag{A2}$$

or

$$s(\mathbf{r}, \mathbf{r}_m) = \mathbf{H}^T \mathbf{X}, \tag{A3}$$

where:

$$\begin{aligned} &\boldsymbol{\lambda} = [\lambda_1, \lambda_2, \mathrm{K}\ , \lambda_M]^T \quad [M \times 1] \\ &\mathbf{b} = [b_1, b_2, \mathrm{K}\ , b_{N_{poly}}]^T \quad [N_{poly} \times 1] \\ &\mathbf{M} = \phi \|\mathbf{r} - \mathbf{r}_m\| \quad [M \times 1] \\ &\mathbf{P} = [p_1 \quad p_2 \quad \Lambda \quad p_{N_{poly}}] \quad [N_{poly} \times 1] \end{aligned} . \tag{A4}$$

Assuming $\mathbf{P} = [1 \quad x \quad y]$, the vectors **H** and **X** in Eq. (A3) become:

$$\begin{aligned} &\mathbf{H} = [\phi \|\mathbf{r} - \mathbf{r}_1\| \quad \phi \|\mathbf{r} - \mathbf{r}_2\| \quad \Lambda \quad \phi \|\mathbf{r} - \mathbf{r}_M\| \quad 1 \quad x \quad y] \\ &\mathbf{X} = [\lambda_1 \quad \lambda_2 \quad \Lambda \quad \lambda_M \quad b_1 \quad b_2 \quad b_3]^T \end{aligned} . \tag{A5}$$

The coefficients λ_m and b_j in Eq. (A1) are determined by enforcing the interpolation pass through all M scattered nodal points within the influence domain Ω

$$s(\mathbf{r}_m) = \mathbf{f}_m \quad m = 1, \mathrm{K}\ , M \tag{A6}$$

with $\mathbf{f}_m$ the values of the nonlinear parameters at each receiver's position M on the damaged zone. Although the addition of polynomial terms does not improve greatly the accuracy for non-polynomial functions, theoretically studies revealed that there was not guarantee that the interpolating condition could be satisfied without the use of

polynomial terms. Particularly, given a set of nodes $\boldsymbol{r}_m$ and a set of functions f_m, the thin-plate spline is the function $s^*(\mathbf{r})$ that satisfies the interpolator condition $s^*(\mathbf{r}_m) = f_m$ and minimises the integral of the second order derivative squared defined by [39]:

$$s^*(\mathbf{r}) = \arg\min \|s(\mathbf{r})\|, \tag{A7}$$

where

$$\|s(\mathbf{r})\|^2 = \int_{\Re^3} \left(\frac{\partial^2 s(\mathbf{r})}{\partial x^2} \right)^2 + \left(\frac{\partial^2 s(\mathbf{r})}{\partial y^2} \right)^2 + \left(\frac{\partial^2 s(\mathbf{r})}{\partial z^2} \right)^2 + 2\left(\frac{\partial^2 s(\mathbf{r})}{\partial x \partial y} \right)^2 + 2\left(\frac{\partial^2 s(\mathbf{r})}{\partial x \partial z} \right)^2 + 2\left(\frac{\partial^2 s(\mathbf{r})}{\partial y \partial x} \right)^2 d\mathbf{r},$$

and $\|s(\boldsymbol{r})\|^2$ is a measure of the energy in the second order derivative of $s(\mathbf{r})$. Moreover, in order to ensure a unique solution of the resulting system of linear equations, the following orthogonality or side condition must be satisfied:

$$\sum_{m=1}^{M} x_m \lambda_m = \sum_{m=1}^{M} y_m \lambda_m = 0. \tag{A8}$$

More generally, if the polynomial in Eq. (A1) is of degree *k*, then the side conditions imposed on the coefficients of the basis functions are

$$\sum_{m=1}^{M} \lambda_m q(\mathbf{r}_m) = 0 \tag{A9}$$

for all polynomials *q* of degree at most *k*. Eqs. (A6) and (A9) lead to a linear system to solve for the coefficients that specify the RBF:

$$\begin{bmatrix} \boldsymbol{A} & \boldsymbol{P} \\ \boldsymbol{P}^T & \boldsymbol{0} \end{bmatrix} \begin{bmatrix} \boldsymbol{\lambda} \\ \boldsymbol{b} \end{bmatrix} = \begin{bmatrix} \boldsymbol{f} \\ \boldsymbol{0} \end{bmatrix} \tag{A10}$$

where

$$\mathbf{A} = \phi\left\|\mathbf{r}_m - \mathbf{r}_j\right\| \quad [M \times M],$$
$$\mathbf{P} = \begin{bmatrix} 1 & x_1 & y_1 \\ 1 & x_2 & y_2 \\ \mathrm{M} & \mathrm{M} & \mathrm{M} \\ 1 & x_M & y_M \end{bmatrix} \quad [M \times N_{poly}], \tag{A11}$$

and the vector of function values at each node is:

$$\mathbf{f} = [f_1, f_2, f_3, \mathrm{K}\ , f_M]^T \quad [M \times 1]. \tag{A12}$$

Eq. (A10) can also be rewritten as

$$\boldsymbol{GX} = \boldsymbol{Q}, \tag{A13}$$

with:

$$\mathbf{G} = \begin{bmatrix} \phi\left\|\mathbf{r}_1 - \mathbf{r}_1\right\| & \phi\left\|\mathbf{r}_1 - \mathbf{r}_2\right\| & \Lambda & \phi\left\|\mathbf{r}_1 - \mathbf{r}_M\right\| & 1 & x_1 & y_1 \\ \phi\left\|\mathbf{r}_2 - \mathbf{r}_1\right\| & \phi\left\|\mathbf{r}_2 - \mathbf{r}_2\right\| & \Lambda & \phi\left\|\mathbf{r}_2 - \mathbf{r}_M\right\| & 1 & x_2 & y_2 \\ \mathrm{M} & \mathrm{M} & \mathrm{O} & \mathrm{M} & \mathrm{M} & \mathrm{M} & \mathrm{M} \\ \phi\left\|\mathbf{r}_M - \mathbf{r}_1\right\| & \phi\left\|\mathbf{r}_M - \mathbf{r}_2\right\| & \Lambda & \phi\left\|\mathbf{r}_M - \mathbf{r}_M\right\| & 1 & x_M & y_M \\ 1 & 1 & \Lambda & 1 & 0 & 0 & 0 \\ x_1 & x_2 & \mathrm{O} & x_M & 0 & 0 & 0 \\ y_1 & y_2 & \Lambda & y_M & 0 & 0 & 0 \end{bmatrix}. \tag{A14}$$

$$\mathbf{Q} = [f_1, f_2, f_3, \mathrm{K}\ , f_M, 0, 0, 0, 0]^T$$

RBF are very effective for interpolating scattered data as the associated system of linear equations is guaranteed to be invertible under very simple conditions on the locations of the data points. Unique solution of Eq. (A13) yields:

$$\boldsymbol{X} = \boldsymbol{G}^{-1}\boldsymbol{Q}. \tag{A15}$$

Hence, the values $\boldsymbol{f}_m$ in all the points within the influence domain Ω with coordinates $\mathbf{r}$ that were obtained through an interpolation with RBF, can be derived by substituting Eq. (A15) in Eq. (A2) as follows:

$$s(\mathbf{r}, \mathbf{r}_m) = \mathbf{H}^T\mathbf{G}^{-1}\mathbf{Q}. \tag{A16}$$

References

[1] Scarselli, G., Maffezzoli, A., Castorini, E., Taurino, A., "Vibrational analysis of aerospace composite components for production defects and operating damage detection," Proceedings of 9th International Conference on Composite Science and Technology (ICCST9), 811-819, (2013).

[2] Ciampa F, Meo M. "Impact detection in anisotropic materials using a time reversal approach". Structural Health Monitoring **11** (1), 43-49 (2012).

[3] Ciampa, F., Boccardi, S., Meo, M. Factors affecting the imaging of impact location with inverse filtering and diffuse wave fields. Journal of Intelligent Material Systems and Structures, doi: 10.1177/1045389X15596622, (2015).

[4] Moustafa, A., Niri, E. D., Farhidzadeh, A., & Salamone, S. "Corrosion monitoring of post-tensioned concrete structures using fractal analysis of guided ultrasonic waves", Structural Control and Health Monitoring, **21**(3), 438-448, (2014).

[5] Michaels, J.-E. and Michaels, T.-E. "Guided wave signal processing and image fusion for in situ damage localization in plates", *Wave Motion **44***, 482-492, (2007).

[6] Michaels, J.-E and Michaels, T.-E. "Damage Localization in Inhomogeneous Plates Using a Sparse Array of Ultrasonic Transducers", *AIP Conference Proceedings 894*, 846-853, (2007).

[7] Lin, X. and Yuan, F.-G. "Damage detection of a plate using migration technique", *Journal of Intelligent Material Systems and Structures*, **12**(*7*), 469–482, (2001).

[8] Wang, L. and Yuan, F.-G. "Damage Identification in a Composite Plate using Prestack Reverse-time Migration Technique", *Structural Health Monitoring* **4** (3), 195-211, (2005).

[9] de Lima, W.J.-N and Hamilton M.-F., “Finite-amplitude waves in isotropic elastic plates”, J. Sound Vib. **265**, 819 (2003).

[10] Amura, M., Meo, M., “Prediction of residual fatigue life using nonlinear ultrasound,” Smart Materials and Structures, **21** (4), 045001, (2012).

[11] Zaitsev, V., Sas, P., “Nonlinear response of a weakly damaged metal sample: a dissipative modulation mechanism of vibro-acoustic interaction,”. J. Vib. Control. 6:803–22 (2000).

[12] Yelve, N. P., Mitra, M., & Mujumdar, P. M. “Spectral damage index for estimation of breathing crack depth in an aluminum plate using nonlinear Lamb wave”, Structural Control and Health Monitoring, **21**(5), 833-846, (2014).

[13] Scarselli, G., Ciampa, F., Ginzburg, Meo, M. “Non-destructive testing techniques based on nonlinear methods for assessment of debonding in single lap joints”, Proc. SPIE 9437, Structural Health Monitoring and Inspection of Advanced Materials, Aerospace, and Civil Infrastructure 2015, 943706, doi:10.1117/12.2085654, (2015).

[14] Kyung-Young Jhang, “Applications of Nonlinear Ultrasonics to the NDE of Material Degradation,” IEEE transactions on ultrasonics, ferroelectrics, and frequency control **47**(3):540–8, (2000).

[15] Landau, L. D., Lifshitz, E. M., [Theory of Elasticity], Chap. III, Pergamon, Oxford, (1986).

[16] Meo, M., Zumpano, G., “Nonlinear elastic wave spectroscopy identification of impact damage on a sandwich plate,” Composite Structures, **71**: 469–474, (2005).

[17] Bruno, C.L.E., Gliozzi, A.S., Scalerandi, M. Antonaci, P., "Analysis of elastic nonlinearity using the Scaling Subtraction Method", *Phys. Rev. B, **79*** (6) 064108(1–13), (2009).

[18] Dos Santos, S., Vejvodova, S. and Prevorovsky, Z., "Nonlinear signal processing for ultrasonic imaging of material complexity", *Proceedings of the Estonian Academy of Sciences*, ***59*** (2), 108-117, (2010).

[19] Zumpano, G., Meo, M., "Damage localization using transient non-linear elastic wave spectroscopy on composite structures," International Journal of Non-Linear Mechanics, **43**: 217 – 230, (2008).

[20] Solodov, I., Bai, J. and Busse G., "Resonant ultrasound spectroscopy of defects: case study of flat-bottomed holes", *J Appl Phys* **113**:223512 (2013)

[21] Ciampa, F., Meo, M., "Nonlinear elastic imaging using reciprocal time reversal and third order symmetry analysis," J. Acoust. Soc. Am. **131** (6), 4316-4323, (2012).

[22] Ciampa, F., Meo, Nonlinear imaging method using second order phase symmetry analysis and inverse filtering. Journal of Nondestructive Evaluation, **34** (2), 1-6, (2015).

[23] Gelman, L., White, P., and Hammond, J., "Fatigue Crack Diagnostics: A Comparison of the Use of the Complex Bicoherence and Its Magnitude", *Mechanical Systems and Signal Processing*, **19**(4):913-918, (2005).

[24] Ciampa, F., Scarselli, G., Pickering, S., Meo, M. Nonlinear elastic wave tomography for the imaging of corrosion damage. Ultrasonics, **62**, 147-155, (2015).

[25] Carr, J.-C., Beatson, R.-K., Cherrie, J.-B., Mitchell, T.-J., Fright, W.-R., McCallum, B.-C, Evans, T.-R., "Reconstruction and Representation of 3D Objects

with Radial Basis Functions," SIGGRAPH' 01, Proceedings of the 28th annual conference on Computer graphics and interactive techniques, 67-76, (2001).

[26] Ferreira A.J.-M., "A formulation of the multiquadric radial basis function method for the analysis of laminated composite plates", Compos. Struct., **59** , pp. 385–392, (2003).

[27] de Boer, A. van der Schoot, M.-S., Bijl, H. "Mesh deformation based on radial basis function interpolation", Comput Struct, **85** (11–14), pp. 784–795, (2007).

[28] Fackrell, J. W. A., White, P. R., Hammond, J. K., Pinnington, R. J., and Parsons, A. T., "The interpretation of the bispectra of vibration signals - I. Theory", Mechanical System and Signal Processing **9**(3), 257–266, (1995).

[29] Kim, Y.-C., Powers, E.-J., "Digital Bispectral Analysis and its Applications to Nonlinear Wave Interactions," IEEE Transactions on Plasma Science, Ps-**7**, 120-131 (1979).

[30] Nikias, C.-L., Raghuveer, M.-R., "Bispectrum estimation: a digital signal processing framework," Proc. IEEE **75**, 869-91 (1987).

[31] Fackrell, J. W.-A., McLaughlin, S. "The Higher Order Statistics of Speech Signals," Proceedings of the IEE Colloquium on Techniques in Speech Signal Processing, London, Digest No. 1994/138, 7/1-7/6 (1994).

[32] Idjimarene, S., Bentahar, M., El Guerjouma, R., Scalerandi, M., "Effects of experimental configuration on the detection threshold of hysteretic elastic nonlinearity", *Ultrasonics*, vol. **54** (7), pp. 1861-1867, (2014).

[33] Ostrovsky, L., Johnson, P.-A., "Dynamic nonlinear elasticity in geomaterials," Riv. Nuovo Cim. **24**, 1−46, (2001).

[34] Fackrell, J.W.-A., White, P.-R., Hammond, J.-K., Pinnington, R.-J., and Parsons, A.-T., 'The interpretation of the bispectra of vibration signals - II. Experimental results and applications', Mechanical System and Signal Processing **9**(3), 267–274, (1995).

[35] Pecorari, C., "Nonlinear interaction of plane ultrasonic waves with an interface between rough surfaces in contact", J. Acoust. Soc. Am. **113** (6), 3065-72 (2003).

[36] Ciampa, F., Meo, M., "Impact localization on a composite tail rotor blade using an inverse filtering approach", *Journal of Intelligent Material Systems and Structures*, vol. **25** (15), pp. 1950-1958, (2014).

[37] Lee, Y.-J. and Yoon, J., "Nonlinear image upsampling method based on radial basis function interpolation", IEEE Trans. Image Process., vol. **19**, n. 10, pp.2682 - 2692, (2010).

[38] Yu, H., Xie, T.-T., Paszczynski, S., and Wilamowski, B.-M., "Advantages of radial basis function networks for dynamic system design", *IEEE Trans. Indust. Electron.*, vol. **58**, n. 12, pp.5438 -5450, (2011).

[39] Orr, M.J.-L., "Regularization in the selection of radial basis function centers", Neural Computat., vol. **7**, no. 3, pp.606 -623 (1995).